ELSEVIER

International Journal of Heat and Fluid Flow 21 (2000) 11–21

International Journal of
HEAT AND
FLUID FLOW

www.elsevier.com/locate/ijhff

Axial steady free surface jet impinging over a flat disk with discrete heat sources

Antonio J. Bula [a], Muhammad M. Rahman [a,*], John E. Leland [b]

[a] *Department of Mechanical Engineering, University of South Florida, 4202 East Fowler Ave, ENB 118, Tampa, FL 33620-5350, USA*
[b] *Aero Propulsion and Power Directorate, Air Force Research Laboratory, Wright Patterson AFB, OH 45433, USA*

Received 5 January 1999; accepted 29 June 1999

Abstract

A free jet of high Prandtl number fluid impinging perpendicularly on a solid substrate of finite thickness containing small discrete heat sources on the opposite surface has been analyzed. Both solid and fluid regions have been modeled and solved as a conjugate problem. Equations for the conservation of mass, momentum, and energy were solved taking into account the transport processes at the solid–liquid and liquid–gas interfaces. The shape and location of the free surface (liquid–gas interface) was determined iteratively as a part of the solution process by satisfying the kinematic condition as well as the balance of normal and shear forces at this interface. The number of elements in the fluid and solid regions were determined from a systematic grid-independence study. A non-uniform grid distribution was used to adequately capture large variations near the solid–fluid interface. Computed results included velocity, temperature, and pressure distributions in the fluid, and the local and average heat transfer coefficients at the solid–fluid interface. Computations were carried out to investigate the influence of different operating parameters such as jet velocity, heat flux, plate thickness, and plate material. Numerical results were validated with available experimental data. It was found that the local heat transfer coefficient is maximum at the center of the disk and decreases gradually with radius as the flow moves downstream. The thickness of the disk as well as the location of discrete sources showed strong influence on the maximum temperature and the average heat transfer coefficient. © 2000 Elsevier Science Inc. All rights reserved.

Keywords: Jet impingement; Electronics cooling; Discrete heat sources

Notation

b	thickness of the disk [m]
c_p	specific heat at constant pressure [kJ/kg K]
g	acceleration due to gravity [m/s^2]
h	heat transfer coefficient [W/m^2 K]
H_n	height of the nozzle from the disk [m]
k	thermal conductivity [W/m K]
n	coordinate normal to the free surface [m]
Nu	Nusselt number $[hr_0/k_f]$
p	pressure [Pa]
q	heat flux [W/m^2]
q_0	total heat transfer rate [W]
r	radial coordinate [m]
r_n	radius of the nozzle [m]
r_0	radius of the disk [m]
Re	Reynolds number, $2r_n\upsilon_j/\nu_f$
T	temperature [K]
$\bar{T}$	average temperature [K]
T_j	jet temperature [K]
υ_j	jet velocity [m/s]
υ_r	radial velocity [m/s]
υ_t	velocity along the free surface [m/s]
υ_z	axial velocity [m/s]
z	axial coordinate [m]

Greek

δ	liquid film thickness [m]
μ	dynamic viscosity of fluid [kg/ms]
ρ	density [kg/m^3]
σ	surface tension coefficient [N/m]

Subscripts

atm	atmospheric condition
av	average
f	fluid
int	solid–fluid interface
s	solid
w	bottom of the disk

1. Introduction

Liquid jets can be classified as submerged or free surface. A submerged jet is formed when a liquid jet is discharged into the same liquid medium. A free surface jet is formed when a liquid jet is discharged into a gaseous (or different liquid) medium.

---

[*] Corresponding author.
E-mail address: rahman@eng.usf.edu (M.M. Rahman).

0142-727X/00/$ - see front matter © 2000 Elsevier Science Inc. All rights reserved.
PII: S0142-727X(99)00054-5

A vast amount of literature exists on free surface as well as submerged (including confined) jets. Examples of books and review articles include Rajaratnam (1976), Martin (1977), Rodi (1982) and Polat et al. (1989).

An interesting application of liquid jets impinging over a surface is for the cooling of microelectronics. Wang et al. (1990) applied a previously developed analytical solution to predict the surface temperature and heat flux distributions of a chip cooled by a laminar impinging free surface FC-77 liquid or water jet. A uniform heat flux distribution at the heated surface of the chip was assumed. They presented results for two different nozzle diameters. Wadsworth and Mudawar (1990) performed an experiment to investigate single-phase heat transfer from a simulated chip to a two-dimensional free surface jet of dielectric fluid FC-72. They concluded that the rectangular jets are well suited for the cooling of high power density discrete heat sources. Schaffer et al. (1991) presented the results of an experimental study measuring the average heat transfer coefficient for discrete sources located under a liquid jet issuing from a rectangular slot. The experiment was conducted for heat sources mounted on a channel (submerged jet). Besserman et al. (1991) presented a numerical simulation of an axisymmetric, laminar jet impingement cooling of a circular heat source. The simulation includes the effect of the discharge fluid when redirected 180° to an annular exit. Their results demonstrated that the flow is strongly influenced by two recirculation zones near the exit and at the corner of the outside annulus. For nozzle parabolic velocity profile, the local Nusselt number presented a maximum at the stagnation point. Womac et al. (1993) obtained experimental data for liquid jet impingement cooling of small square heat sources resembling integrated circuit chips. Both free surface and submerged jet configuration were studied for a range of velocities, nozzle diameters and nozzle-to-heater distance. Two different liquids, water and FC-77, were used as coolants. Womac et al. (1994) carried out an experiment to investigate single-phase heat transfer from a heat source to an array of free surface and submerged jets. They found that for a constant volumetric flow rate, the heat transfer for submerged jets exceeded or were approximately equal to those for the free surface jets. The average heat transfer coefficient increased with reduction in nozzle diameter. Rice and Garimella (1994) reported an experimental study to determine the local heat transfer coefficient distribution for a submerged liquid jet impinging perpendicularly on a small, square heat source simulating an electronic cooling situation. They concluded that the local heat transfer coefficient at the stagnation point was independent of the nozzle-to-plate distance for small nozzle diameters, and for distances over 5 nozzle diameters the stagnation heat transfer coefficient decreased. Secondary peaks were observed as the fluid moved away from the stagnation point. Maddox and Bar-Cohen (1994) carried out a study to help design a jet impingement cooling system in attaining the targeted thermal performance while considering the available liquid pressure, liquid flow rate, and pumping power, as well as jet plate manufacturing and maintenance constraints. Garimella and Rice (1995) experimentally investigated the local heat transfer from a small heat source to a normally impinging axisymmetric and submerged liquid jet, in confined and unconfined configurations. Secondary peaks were more pronounced at smaller (confined) spacings and large nozzle diameters for a given Reynolds number. Correlations were presented for the average heat transfer coefficient and the Nusselt number.

From the above literature review, it appears that most jet impingement cooling studies involving discrete heat sources used either water or a fluorinert liquid as the cooling medium. In addition, the variation of fluid properties with temperature has not been taken into account in any previous numerical work, and has been assumed to be negligible in most analytical work. Although a poor heat transfer fluid, lubricating oil is an attractive coolant for aircraft applications because it is generally in close proximity to the electrical generating equipment. It is also pre-existing in the aircraft and therefore does not require flight qualification, new maintenance procedures, additional inventory space and logistics procedures, or additional environmental protection guidelines. These advantages translate into greatly reduced operational costs, which may far overweigh the loss in cooling efficiency. Lubricating oils are generally known for their high Prandtl number and strong dependence of viscosity on temperature. Alternately, air-cooling is generally inadequate or undesirable because of the additional drag imposed by ram air heat exchangers. Therefore, the investigation of jet impingement heat transfer for high Prandtl number fluids taking into account the effects of property variation with temperature is of great importance to the military and commercial aircraft industry, and is expected to be a valuable contribution to the state-of-the-art of jet impingement cooling system design.

2. Mathematical model

Consider an axisymetric jet discharging from a nozzle and impinging perpendicularly at the center of a solid circular disk heated by discrete sources as shown in Fig. 1. If the fluid is considered to be incompressible and its properties (density, viscosity, thermal conductivity and specific heat) are dependent on temperature, the equations describing the conservation of mass, momentum and energy in cylindrical coordinates can be written as (Burmeister, 1993):

$$\frac{1}{r}\frac{\partial}{\partial r}(\rho_{\mathrm{f}} r \upsilon_{\mathrm{r}}) + \frac{\partial}{\partial z}(\rho_{\mathrm{f}} \upsilon_z) = 0, \tag{1}$$

$$\rho_{\mathrm{f}}\left(\upsilon_{\mathrm{r}}\frac{\partial \upsilon_{\mathrm{r}}}{\partial r} + \upsilon_z\frac{\partial \upsilon_{\mathrm{r}}}{\partial z}\right) = -\frac{\partial p}{\partial r} + \frac{1}{r}\frac{\partial}{\partial r}\left[\frac{2}{3}\mu r\left(2\frac{\partial \upsilon_{\mathrm{r}}}{\partial r} - \frac{\upsilon_{\mathrm{r}}}{r} - \frac{\partial \upsilon_z}{\partial z}\right)\right] + \frac{\partial}{\partial z}\left[\mu\left(\frac{\partial \upsilon_{\mathrm{r}}}{\partial z} + \frac{\partial \upsilon_z}{\partial r}\right)\right], \tag{2}$$

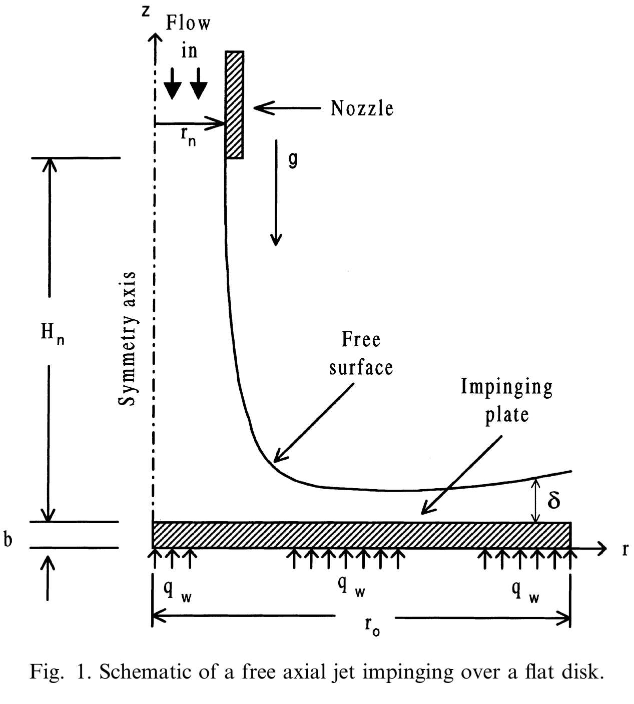

Fig. 1. Schematic of a free axial jet impinging over a flat disk.

$$\rho_f\left(v_r\frac{\partial v_z}{\partial r}+v_z\frac{\partial v_z}{\partial z}\right)=-\rho_f g-\frac{\partial p}{\partial z}+\frac{1}{r}\frac{\partial}{\partial r}\left[\mu r\left(\frac{\partial v_r}{\partial z}+\frac{\partial v_z}{\partial r}\right)\right]+\frac{\partial}{\partial z}\left[\frac{2}{3}\mu\left(2\frac{\partial v_z}{\partial z}-\frac{v_r}{r}-\frac{\partial v_r}{\partial r}\right)\right], \tag{3}$$

$$\begin{aligned}\rho_f\left(v_r\frac{\partial(c_{p_f}T_f)}{\partial r}+v_z\frac{\partial(c_{p_f}T_f)}{\partial z}\right)&=\left[\frac{1}{r}\frac{\partial}{\partial r}\left(k_f r\frac{\partial T_f}{\partial r}\right)+\frac{\partial}{\partial z}\left(k_f\frac{\partial T_f}{\partial z}\right)\right]+\left(v_z\frac{\partial p}{\partial z}+v_r\frac{\partial p}{\partial r}\right)\\&\quad+\mu_f\left\{2\left[\left(\frac{\partial v_r}{\partial r}\right)^2+\left(\frac{v_r}{r}\right)^2+\left(\frac{\partial v_z}{\partial z}\right)^2\right]\right.\\&\quad\left.+\left(\frac{\partial v_r}{\partial z}+\frac{\partial v_z}{\partial r}\right)^2-\frac{2}{3}\left[\frac{\partial v_r}{\partial r}+\frac{v_r}{r}+\frac{\partial v_z}{\partial z}\right]^2\right\}.\end{aligned} \tag{4}$$

Considering variable thermal conductivity, the equation describing the conservation of energy inside the solid can be written as

$$\frac{1}{r}\frac{\partial}{\partial r}\left(k_s r\frac{\partial T_s}{\partial r}\right)+\frac{\partial}{\partial z}\left(k_s\frac{\partial T}{\partial z}\right)=0. \tag{5}$$

Eqs. (1)–(5) are subjected to the following boundary conditions:

$$\text{At } r=0,\quad 0\leqslant z\leqslant b:\quad \frac{\partial T_s}{\partial r}=0, \tag{6}$$

$$\text{At } r=0,\quad b\leqslant z\leqslant H_n:\quad v_r=0,\quad \frac{\partial v_z}{\partial r}=0,\quad \frac{\partial T_f}{\partial r}=0, \tag{7}$$

$$\text{At } r=r_0,\quad 0\leqslant z\leqslant b:\quad \frac{\partial T_s}{\partial r}=0, \tag{8}$$

$$\text{At } r=r_0,\quad b\leqslant z\leqslant \delta:\quad p=0,\quad \frac{\partial T_f}{\partial r}=0, \tag{9}$$

$$\text{At } z=b:\quad T_s=T_f,\ v_r=0,\ v_z=0,\ k_s\frac{\partial T_s}{\partial z}=k_f\frac{\partial T_f}{\partial z}, \tag{10}$$

$$\begin{aligned}&\text{At } z=b+H_n,\quad 0\leqslant r\leqslant r_n:\\&v_r=0,\quad v_z=-v_j,\quad T_f=T_j,\end{aligned} \tag{11}$$

$$\begin{aligned}&\text{At } z=\delta,\quad r_n<r<r_0:\\&\frac{d\delta}{dr}=\frac{v_z}{v_r},\quad p=p_{atm}-\frac{\sigma(d^2\delta/dr^2)}{\left[1+(d\delta/dr)^2\right]^{3/2}},\\&\frac{\partial v_t}{\partial n}=0,\quad \frac{\partial T_f}{\partial n}=0.\end{aligned} \tag{12}$$

Eq. (12) essentially indicate the kinematic condition, balance of normal forces, balance of shear forces, and adiabatic condition at the free surface. These equations were derived from more general equations presented by White (1999). It can be noted that "n" indicates direction normal to the free surface. The frictional resistance and heat transfer to the surrounding gaseous medium have been assumed to be negligible. In order to simulate different positions of the discrete heat sources, the total heat introduced was taken as constant and the heat flux for the discrete sources was changed according to the total heated area. Fig. 2 demonstrates the boundary condition at the bottom of the disk. For the base case, it can be written as:

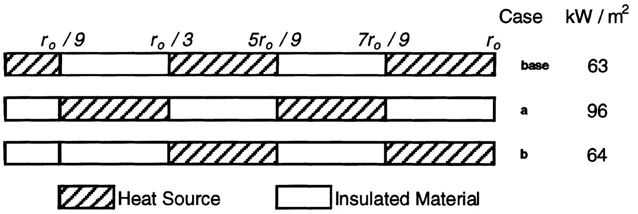

Fig. 2. Different location of heat sources and their heat flux ($q_0 = 1.59$ W).

$$\text{At } z=0,\quad 0<r<(r_0/9):\quad -k_s\frac{\partial T_s}{\partial z}=q_w, \tag{13}$$

$$\text{At } z=0,\quad (r_0/9)<r<(r_0/3):\quad \frac{\partial T_s}{\partial z}=0, \tag{14}$$

$$\text{At } z=0,\quad (r_0/3)<r<(5r_0/9):\quad -k_s\frac{\partial T_s}{\partial z}=q_w, \tag{15}$$

$$\text{At } z=0,\quad (5r_0/9)<r<(7r_0/9):\quad \frac{\partial T_s}{\partial z}=0, \tag{16}$$

$$\text{At } z=0,\quad (7r_0/9)<r<r_0:\quad -k_s\frac{\partial T_s}{\partial z}=q_w. \tag{17}$$

The local heat transfer coefficient can be defined as

$$h=\frac{q_{int}}{(T_{int}-T_j)}. \tag{18}$$

The average heat transfer coefficient is obtained according to the following equation

$$h_{av}=\frac{2}{r_0^2(\bar{T}_{int}-T_j)}\int_0^{r_0} hr(T_{int}-T_j)\,dr. \tag{19}$$

It can be noted that local heat transfer coefficient h and interfacial temperature T_{int} are both functions of radial location r. $\bar{T}_{int}$ is the average temperature at the solid–fluid interface. It was calculated by taking the linear average of temperature from $r=0$ to $r=r_0$. The local Nusselt number and the average Nusselt number are calculated according to the following expressions:

$$Nu=\frac{hr_0}{k_f}, \tag{20}$$

$$Nu_{av}=\frac{h_{av}r_0}{k_f}. \tag{21}$$

3. Computation and discussion of results

The governing equations along with the boundary conditions described in Section 2 were solved by using the Galerkin finite element method (Fletcher, 1984). The dependent variables, i.e., velocity, pressure and temperature were interpolated to a set of nodal points that defined the finite element. In each element, the velocity, pressure and temperature fields were approximated which led to a set of equations that defined the continuum. The approach used to model the free surface was to introduce a new degree of freedom at the nodes on the free surface. This degree of freedom represented the position of the free surface. The discretization of governing transport equations and boundary conditions was carried out using the Galerkin formulation. The solution of the resulting algebraic

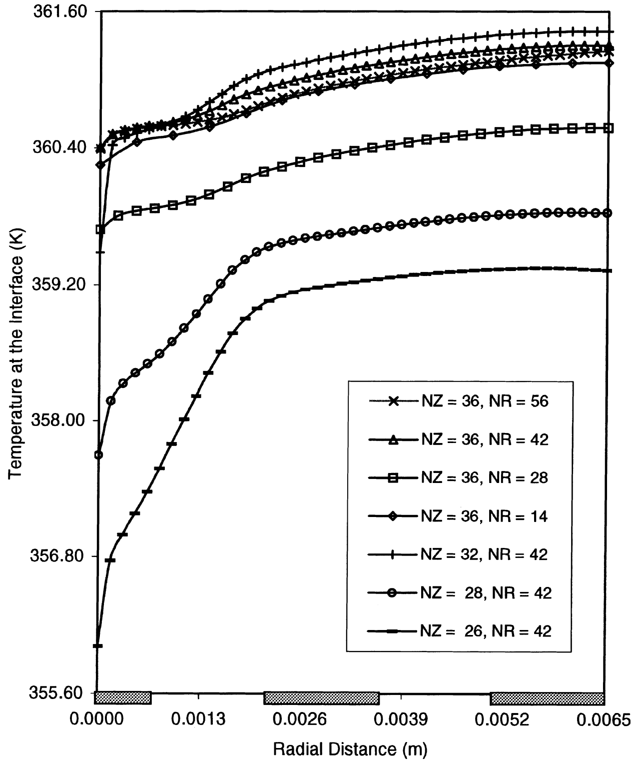

Fig. 3. Interface temperature for different number of elements in axial and radial directions ($Re = 1100$, $T_j = 348$ K, $b = 0.005$ m, $H_n = 0.0085$ m, $r_n = 0.00085$ m, copper plate, $q_w = 63$ kW/m^2).

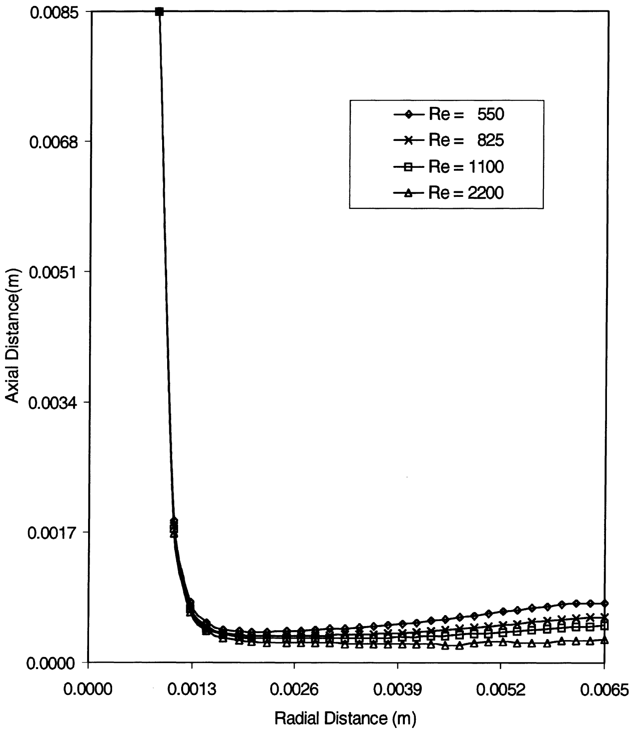

Fig. 4. Free surface height distribution for different Reynolds number ($H_n = 0.0085$ m, $r_n = 0.00085$ m).

equations was carried out using the Newton–Raphson method. Since the solution of the momentum equation required only two out of the three boundary conditions at the free surface, the third condition was used to update the position of the free surface at the end of each iteration step.

Due to large number of iterations required to determine the location of the free surface, the solution was carried out in two steps. First, the computation in the fluid region was carried out solving equations for the conservation of mass and momentum; this resulted in the determination of the velocity field and the free surface height distribution. The drawback of this solution is that because of no heat transfer, the fluid remained isothermal, and therefore properties remained constant. This approximate solution was used as the starting point for the second level of computation where both solid and fluid regions were included and equations for the conservation of mass, momentum and energy were solved simultaneously as a conjugate problem taking into account the variation of properties with temperature. This split level computation procedure greatly reduced the run time for numerical computation. The solution was considered converged when the field values did not change from one iteration to the next, and the sum of residuals for each degree of freedom was less than 1E-08. Except for comparison with Womac et al. (1993), the working fluid used for the present numerical simulation is MIL-7808, a lubrication oil certified for military aircraft. The relevant fluid properties were calculated from the following correlating equations which are valid for 303 $\mathrm{K} < T < 390$ K: $c_p = 903.8 + 3.332T$, $k = 0.18 - 1 \times 10^{-4}T$, $\rho = 1181 - 0.708T$ and $\mu = 0.941 - 5.07 \times 10^{-3}T + 6.87 \times 10^{-6}T^2$. The range of Prandtl number encountered in the present investigation was 48–71. The range of variation of different parameters were: $Re = 550$–2200 and $b = 0.000125$–0.01 m. Three different disk materials and three different heating arrangements were studied. This choice of parameters was essentially driven by applications and past studies of laminar jet impingement heat transfer.

In order to determine the number of elements for accurate numerical solution, computations were performed for several combinations of number of elements in the radial and axial directions covering the solid and fluid regions. The solid–fluid interface temperature for these simulations are plotted in Fig. 3. It was observed that the numerical solution becomes grid independent when the number of divisions in the radial direction is increased over 28 and at least 36 divisions are used in the axial direction. In order to have smooth variation of transport quantities, 42 × 36 divisions in the radial and axial directions were chosen. The size of the elements was different in different regions of the computation domain to accommodate steep velocity and temperature gradients.

Table 1
Comparison between present simulation and Womac et al. (1993) ($T_j = 310$ K, $b = 0.003$ m, $H_n = 0.0165$ m)

Fluid	Re	$T_{max} - T_{min}$ Interface	T_{max} Interface	Nu_{av} Womac et al. (1993)	Nu_{av} Present study	Difference (%)
FC-77	1200	0.084	322.6	181.0	189.0	4.4
Water	1465	0.186	312.9	199.0	197.0	1.0

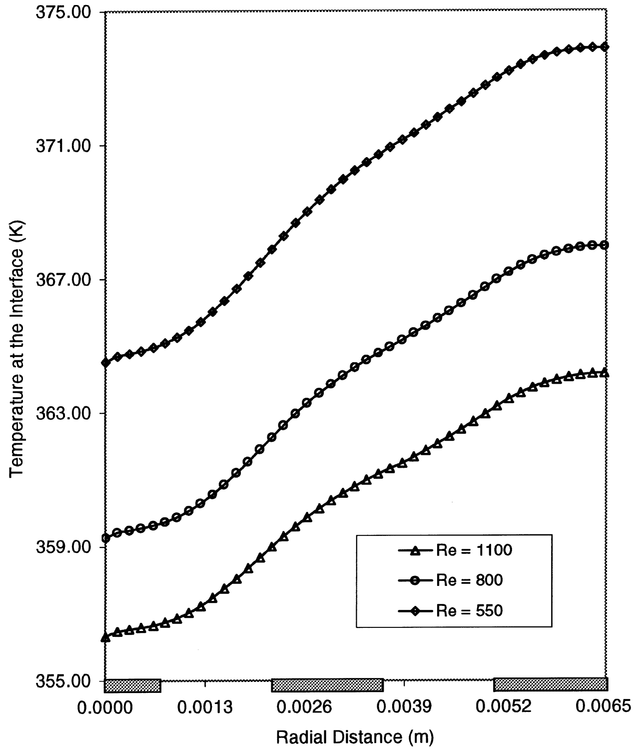

Fig. 5. Temperature at the interface for different Reynolds number ($T_j = 348$ K, $b = 0.000125$ m, $H_n = 0.0085$ m, $r_n = 0.00085$ m, copper plate, $q_w = 63$ kW/m^2).

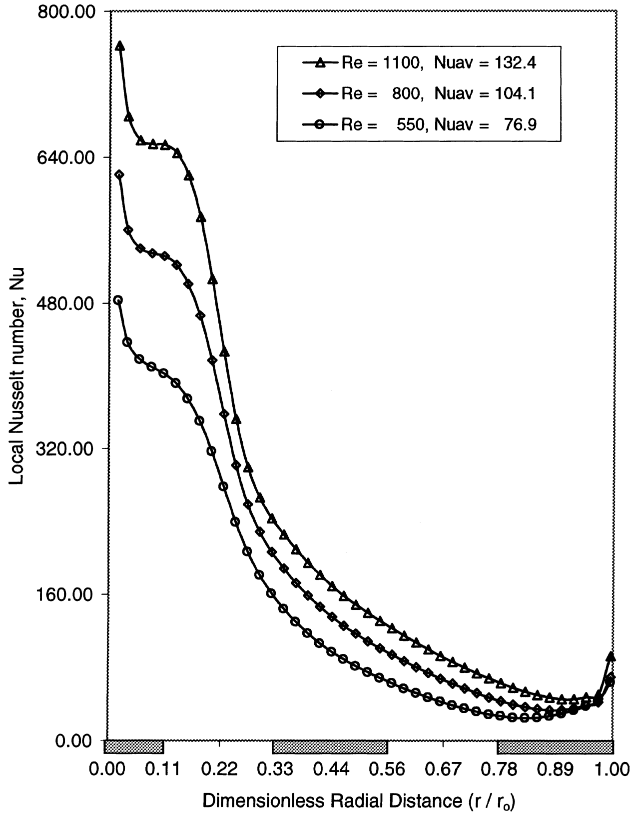

Fig. 6. Local Nusselt number variation for different Reynolds number ($T_j = 348$ K, $b = 0.005$ m, $H_n = 0.0085$ m, $r_n = 0.00085$ m, copper plate, $q_w = 63$ kW/m^2).

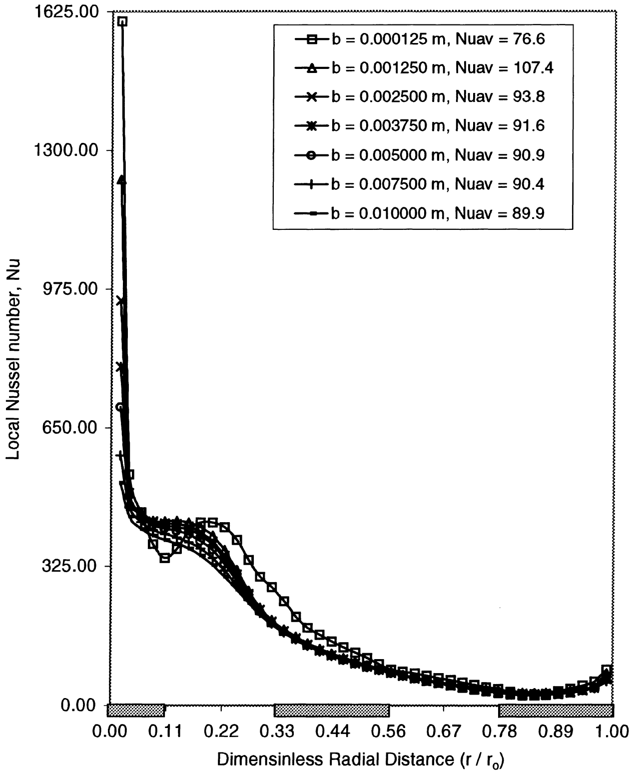

Fig. 7. Local Nusselt number variation for different disk thickness ($Re = 550$, $T_j = 348$ K, $H_n = 0.0085$ m, $r_n = 0.00085$ m, constantan plate, $q_w = 63$ kW/m^2).

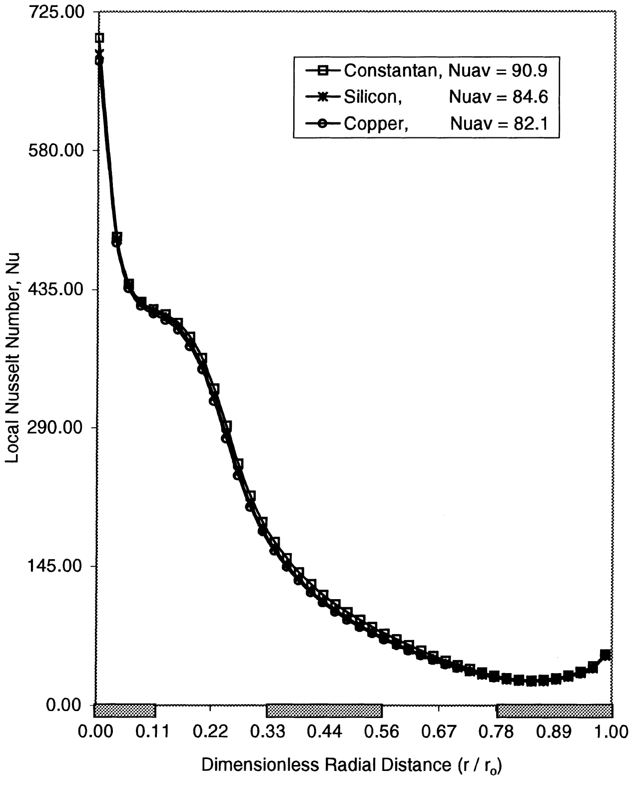

Fig. 8. Local Nusselt number variation for different materials ($Re = 550$, $T_j = 348$ K, $b = 0.005$ m, $H_n = 0.0085$ m, $r_n = 0.00085$ m, $q_w = 63$ kW/m^2).

A comparison between the present numerical simulation and the experimental data obtained by Womac et al. (1993) is presented in Table 1. In order to carry out this comparison, numerical simulations were performed using the appropriate test fluids and heat flux conditions used in the experiment. The table shows a good agreement between the simulation and the experimental data, with a maximum deviation of 4.4%. This comparison validates the results obtained in the present investigation.

Fig. 4 presents the free surface height distribution for different Reynolds number when the jet strikes the center of the disk. It can be seen that the fluid spreads radially as a thin film. For the conditions considered in the present investigation, the flow was supercritical and a hydraulic jump did not occur within the computation domain. It can be observed that the minimum film height occurs at a radius larger than the radius of the nozzle and the film height gradually increases with radius after that location. A smaller thickness is seen at larger Reynolds number because of larger impingement velocity that translates to a larger fluid velocity in the film. From the plot of velocity vectors, it was observed that, due to high viscosity of the working fluid, the boundary layer develops rapidly and the velocity of the fluid decreases as it spreads radially along the disk.

The effect of Reynolds number on the temperature at the interface is observed in Fig. 5. It can be seen that as Reynolds number increases, the temperature at the interface decreases. This is because of larger local fluid velocity, which results in larger rate of heat transfer between the disk and the liquid. The temperature is minimum at the stagnation point. As the fluid moves downstream, the temperature increases. The location where the fluid goes from the stagnation to boundary layer region (transition region) is about $r = r_n$. The temperature distribution shows steeper slope at locations where the heat sources are located, especially in the boundary layer region, $r > r_n$. It is important to notice that as the Reynolds number increases, the maximum-to-minimum temperature difference decreases, ranging from 9.4 to 7.9 K between *Re* of 550 and 1100. This is because of decreasing thermal resistance at the solid–fluid interface.

Fig. 6 presents the effect of Reynolds number on the local Nusselt number. It is observed that the maximum is located at the stagnation point. As the fluid goes through the stagnation zone ($r \leqslant 0.002$ m), the local heat transfer coefficient decreases rapidly. As the fluid reaches the location where the boundary layer starts to develop, an almost uniform Nusselt number zone is attained. After that point, the heat transfer coefficient continues to decrease until reaching the edge of the disk, presenting the pattern of an external flow over a flat surface. As the fluid moves over the last heat source, the heat transfer coefficient slightly increases. This phenomenon was observed in previous studies by Wolf et al. (1990) and Vader et al. (1991). The rise of heat transfer coefficient near the outer edge of the disk is possibly due to transition to turbulence. It should be noted, however, that for the conditions considered in the present investigation, a fully turbulent flow regime could not

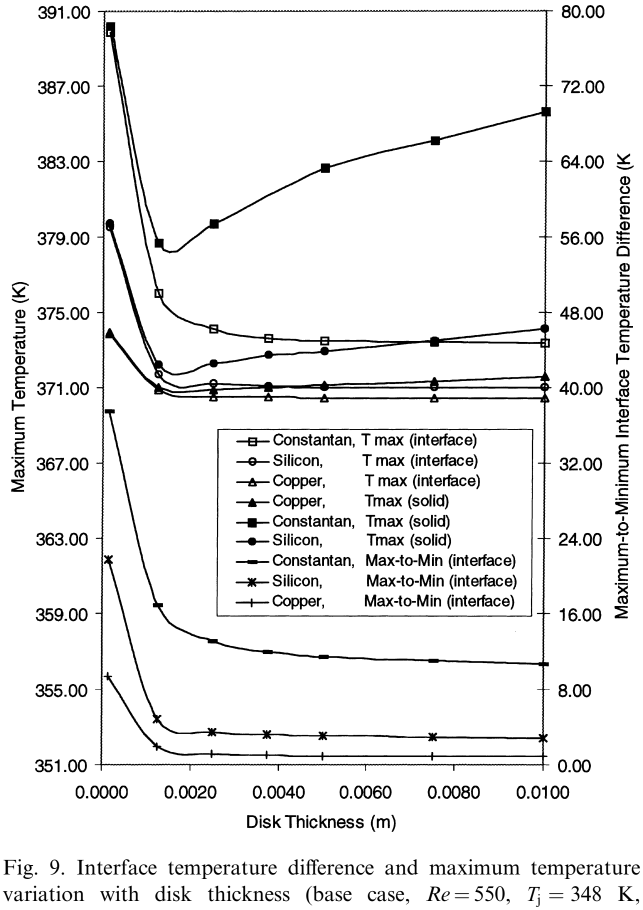

Fig. 9. Interface temperature difference and maximum temperature variation with disk thickness (base case, $Re = 550$, $T_j = 348$ K, $H_n = 0.0085$ m,$r_n = 0.00085$ m, $q_w = 63$ kW/m^2).

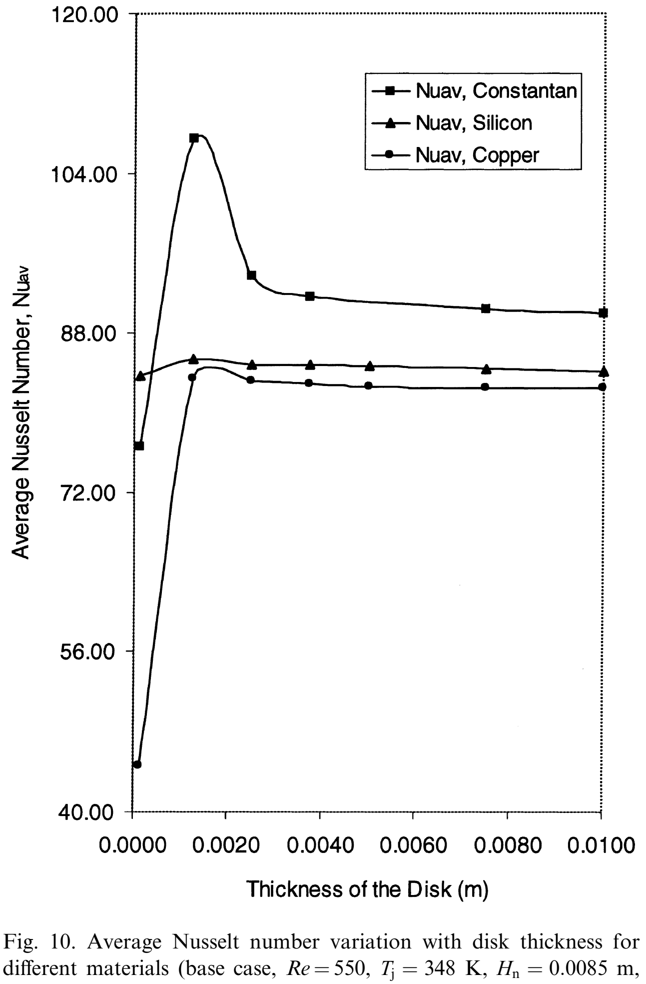

Fig. 10. Average Nusselt number variation with disk thickness for different materials (base case, $Re = 550$, $T_j = 348$ K, $H_n = 0.0085$ m, $r_n = 0.00085$ m, $q_w = 63$ kW/m^2).

be attained. It is important to note that there is a heat source located exactly under the stagnation zone (base case). It can be noted that the maximum (located at the stagnation point), the average, and the uniform zone (attained at the beginning of the boundary layer region) of Nusselt number increase with Reynolds number. The uniform zone appears at the position where the fluid has its minimum thickness and maximum velocity over the plate and this is the reason for the enhancement of the heat transfer process at that location. It can also be associated with the transition of flow from stagnation to boundary layer zone.

Fig. 7 presents the local and average Nusselt number for different disk thicknesses. It is important to notice that the main differences are present at the stagnation region, and as soon as the fluid gets into the boundary layer region, the distributions of Nusselt number for different thickness get close to each other. As the thickness of the disk increases, the temperature distribution at the solid–fluid interface becomes more uniform due to thermal spreading by radial conduction. Therefore, the heat transfer coefficient at the center of the disk decreases. It is noticed that the average Nusselt number increases as the disk thickness increases and reaches a maximum value around 0.00125 m. After this point, the average Nusselt number presents a decreasing trend.

The numerical simulation was carried out for three different disk materials, namely copper, constantan and silicon. Both copper and constantan have been used in previous experimental studies on jet impingement cooling. Silicon was chosen because of its application in electronics fabrication. Fig. 8 shows that the local Nusselt number increases with decrease of thermal conductivity of the disk material. A small difference is seen between copper and silicon because $k_{\mathrm{copper}} = 2.6\ k_{\mathrm{silicon}}$, whereas a somewhat larger difference is seen between copper and constantan because of $k_{\mathrm{copper}} = 17\ k_{\mathrm{constantan}}$. It can be noticed that at large radial locations, the Nusselt number for the different materials practically match each other. The reason why a material with a lower thermal conductivity achieves a higher average Nusselt number lies specifically in its inability to conduct heat. It produces a lower temperature at the stagnation region that reflects as a higher heat transfer coefficient. At the boundary layer region, the difference in temperature for different materials is not significant and the values get closer all the way to the edge of the disk. The local Nusselt number at the center of the disk for different materials were compared with the stagnation Nusselt number correlation developed by Hrycak (1983). It was found that the numerical predictions are within 5–8% of this experimental correlation.

Fig. 9 presents the maximum temperature as well as the difference between the maximum and minimum temperature at the interface, and the maximum temperature inside the solid for the three different disk materials and different disk thicknesses. The control of these temperatures is crucial in the design of electronic packages. It may be noticed that the maximum temperature at the interface decreases with increasing thickness when $b < 0.005$ m, $b < 0.00375$ m, and $b < 0.00125$ m, for constantan, silicon and copper respectively, whereas remains almost constant thereafter. The maximum temperature inside the solid has an interesting behavior. It decreases as the disk thickness increases when $b < 0.00125$ m, $b < 0.002$ m, and $b < 0.0025$ m, for constantan, silicon, and copper respectively, after this point, the temperature increases as the disk thickness increases. This indicates that increasing

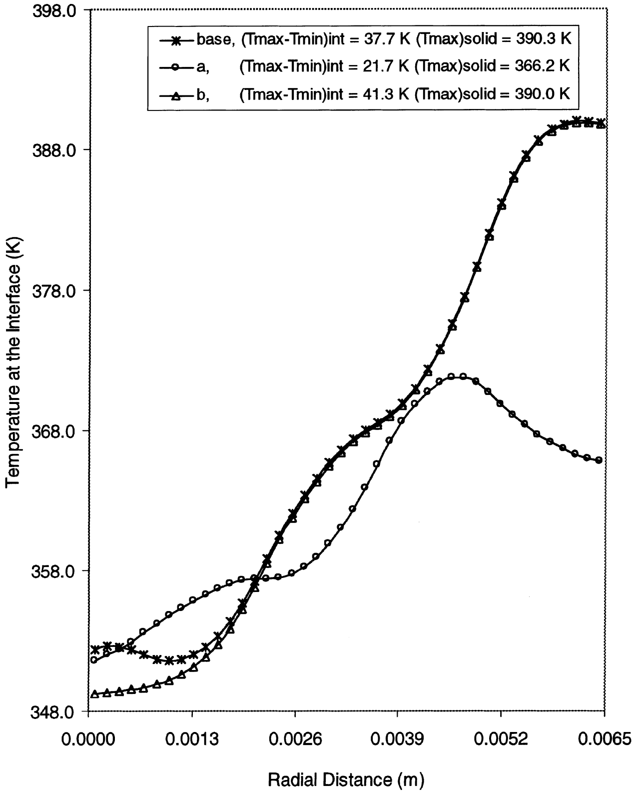

Fig. 11. Temperature distribution at the interface for different positions of heat sources ($Re = 1100$, $T_{\mathrm{j}} = 348$ K, $b = 0.000125$ m, $H_{\mathrm{n}} = 0.0085$ m, $r_{\mathrm{n}} = 0.00085$ m, constantan plate, $q_0 = 1.59$ W).

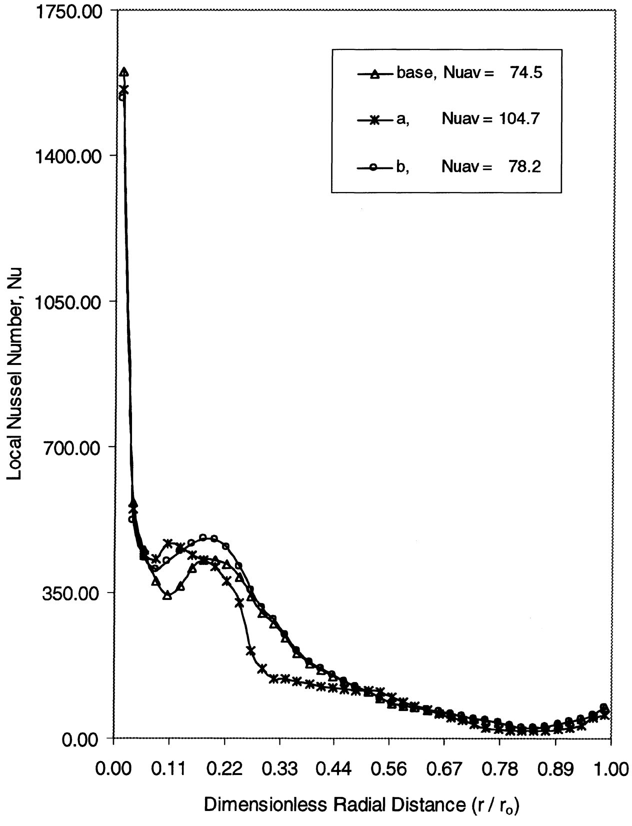

Fig. 12. Local Nusselt number for different heat sources position and heat flux ($Re = 1100$, $T_{\mathrm{j}} = 348$ K, $b = 0.000125$ m, $H_{\mathrm{n}} = 0.0085$ m, $r_{\mathrm{n}} = 0.00085$ m, constantan plate, $q_0 = 1.59$ W).

the wafer thickness beyond a certain limit, depending on the solid material, may not be useful. The choice of the wafer material is however crucial in determining the magnitude of this temperature. As expected, a material with larger thermal conductivity will facilitate a faster rate of heat transfer, and therefore will result in a lower maximum temperature at the interface and inside the solid. The temperature difference at the interface is an indication of the level of temperature non-uniformity at the impingement surface, while the maximum temperature inside the solid indicates the thermal resistance generated by the wafer material. When the disk thickness is negligible, the interface temperature is controlled by the heat flux condition at the heater. However, when an adequate thickness is provided, the interface temperature becomes more uniform because of radial spreading of heat within the solid. The magnitude of maximum to minimum temperature difference is strongly affected by the thermal conductivity of the disk material, decreasing as the disk thermal conductivity increases. The material with lower thermal conductivity results in higher temperature at the interface and inside the solid.

The effect of disk thickness on average Nusselt number for three different materials can be observed in Fig. 10. It shows how the average values of heat transfer coefficient and Nusselt number attain a peak around $b = 0.00125$ m. For $b < 0.00125$ m, the average value of Nusselt number increases as the disk thickness increases. On the other hand, for $b > 0.00125$ m, the average value of Nusselt number slightly decreases as the disk thickness increases. It may be noticed that constantan has a higher value of average heat transfer coefficient than copper or silicon at all disk thicknesses. This is consistent with local variations seen in Fig. 8. For $b < 0.00125$ m, the radial spreading due to conduction increases as the disk thickness increases and there is a better heat distribution at the interface, this creates a better opportunity for the heat to be transferred to the fluid. For $b > 0.00125$ m, the increment in the solid thickness creates more thermal resistance, which ends up crippling the heat transfer process.

In order to study how the position of the discrete heat sources affects the heat transfer phenomenon, it was necessary to input the same power dissipation in the system. For that reason, for different positions, the heat flux varies as shown in Fig. 2. The results for the temperature distribution at the interface and local Nusselt number are presented in Figs. 11 and 12. It may be observed that the location of the heat sources strongly affects the local variation of interface temperature and heat transfer coefficient. The magnitudes of the maximum temperature, maximum-to-minimum temperature difference at the interface, and average Nusselt number are also strongly affected by the location of heat sources. Case (a) is just the opposite of the base case in terms of heater location. For thin disks, as the heat sources are moved closer to the stagnation region, the average heat transfer coefficient increases, presenting maximum values for Case (a). Since no heat source is

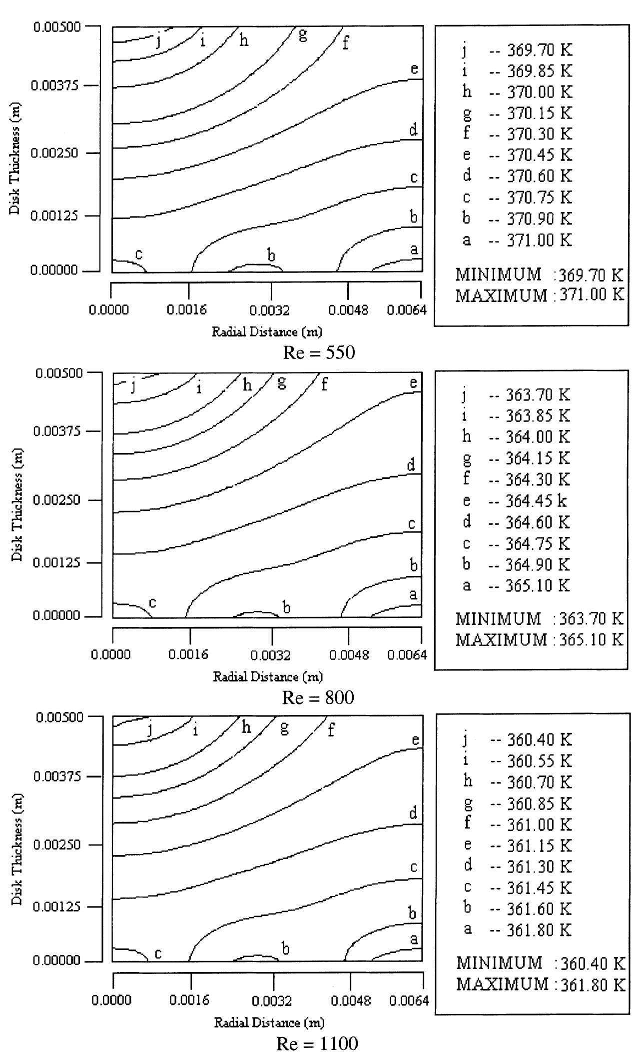

Re = 550

Re = 800

Re = 1100

Fig. 13. Isothermal lines within the disk for different Reynolds number (base case, $T_j = 348$ K, $b = 0.005$ m, $H_n = 0.0085$ m, $r_n = 0.00085$ m, copper plate, $q_w = 63$ kW/m^2).

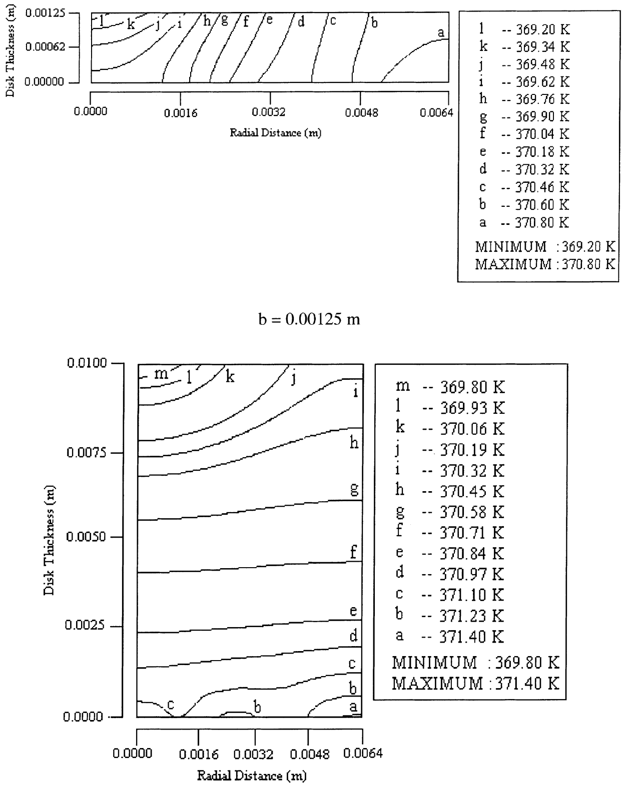

b = 0.00125 m

b = 0.01m

Fig. 14. Isothermal lines within the disk for different disk thickness (base case, $Re = 550$, $T_j = 348$ K, $H_n = 0.0085$ m, $r_n = 0.00085$ m, copper plate, $q_w = 63$ kW/m^2).

present at the exit edge of the disk, the maximum temperature for Case (a) is also lower. This case provides much more uniform temperature at the solid–fluid interface compared to the other two cases. Case (b) is somewhat similar to the base case except that the central heater is removed and heat flux at the other two heaters is increased to provide the same total power dissipation. It may be noticed that because of higher heat flux, T_{max} increased. Case (b), presents the minimum temperature at the interface because of the lack of heat source under the impingement zone (stagnation point).

The temperature contours within the disk for different Reynolds number are presented in Fig. 13. The minimum temperature occurs at the stagnation point, the maximum temperature occurs across the disk at the largest radial location. It is observed that the isothermal lines grow around the heat sources in the lower part of the disk and matches with isotherms concentric with the impingement location in the upper part of the disk. The maximum-to-minimum temperature difference inside the disk remains almost constant (1.3–1.4 K). It is important to notice that Reynolds number does not have a strong effect on the pattern of temperature distribution inside the solid. It seems that this is more controlled by the distribution of heat sources. On the other hand, the magnitude of temperature within the solid is very strongly affected by Reynolds number.

The effect of disk thickness on temperature distribution within the solid is seen in Fig. 14. It can be observed that the temperature becomes more uniform as the disk thickness is increased. It is interesting to notice that when the disk thickness is large, the temperature remains stratified over a part of the disk. The isothermal lines start growing around the heat sources and become parallel to the bottom of the disk indicating an almost one-dimensional heat conduction. However, in regions near the solid–fluid interface, the isothermal lines tend to be concentric around the stagnation point. The effect of non-uniform heat transfer is felt only over a part of the disk. When the disk thickness is small, the temperature contours have entirely different orientation because of strong radial conduction over the entire disk thickness. The temperature difference inside the solid remains almost constant, with a value around 1.6 K.

Fig. 15 shows the temperature distribution inside the disk for the three different materials. For copper and silicon, the temperature is more uniform and the maximum-to-minimum temperature difference is smaller, 1.3 and 4.2 K respectively. For constantan the maximum-to-minimum temperature difference is fairly large (18.2 K) because of much lower thermal conductivity. The shapes of the isotherms are not significantly affected by thermal conductivity.

In order to compare a uniformly heated disk with a discretely heated one (base case), the total heat introduced was uniformly distributed. The temperature at the interface and local Nusselt number are shown in Figs. 16 and 17

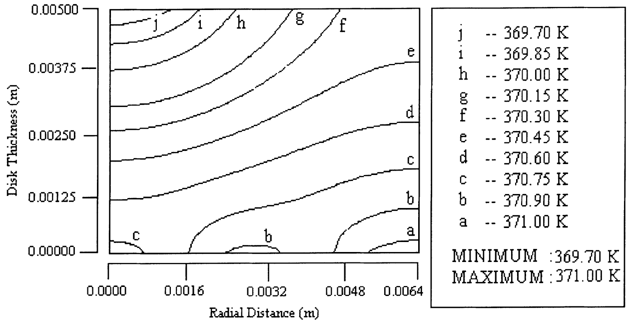

a) Copper

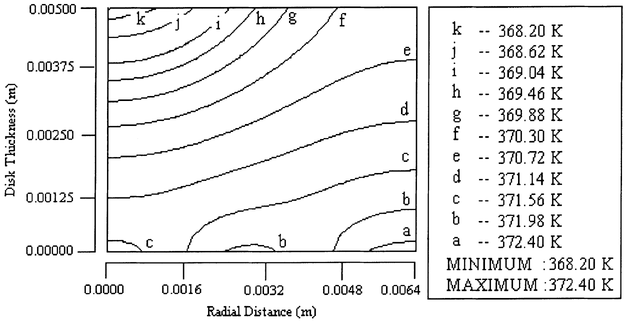

b) Silicon

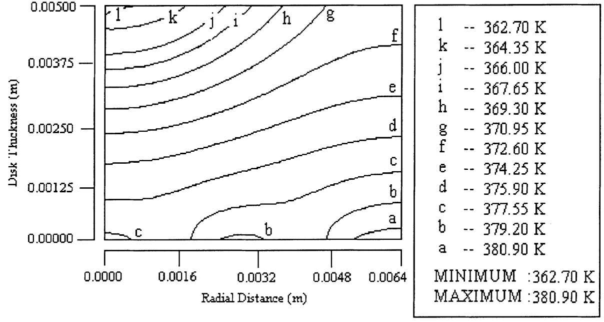

c) Constantan

Fig. 15. Isothermal lines within the disk for different materials (base case, $Re = 550$, $T_j = 348$ K, $b = 0.005$ m, $H_n = 0.0085$ m, $r_n = 0.00085$ m, $q_w = 63$ kW/m^2).

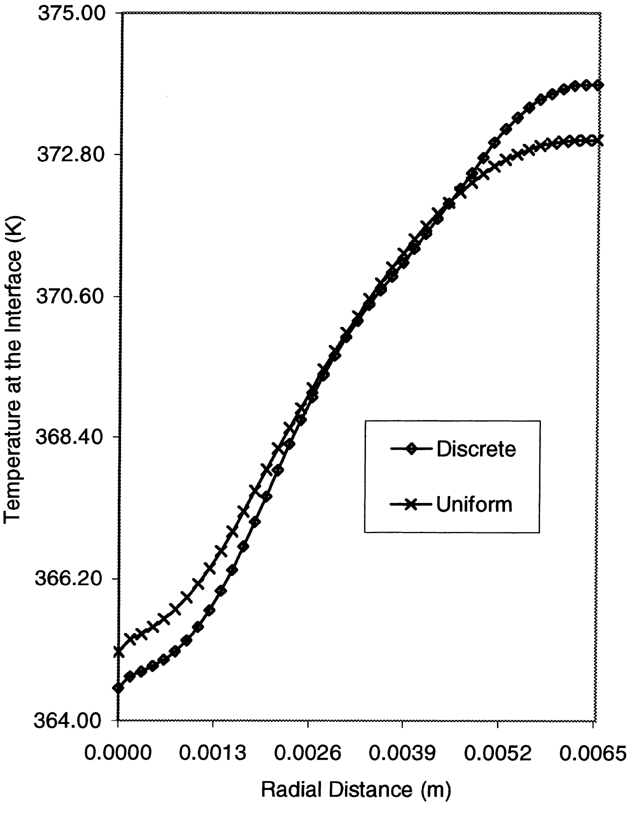

Fig. 16. Temperature distribution at the interface for discrete (base case) and uniform heat flux distribution ($Re = 550$, $T_j = 348$ K, $b = 0.000125$ m, $H_n = 0.0085$ m, $r_n = 0.00085$ m, constantan plate, $q_0 = 1.59$ W).

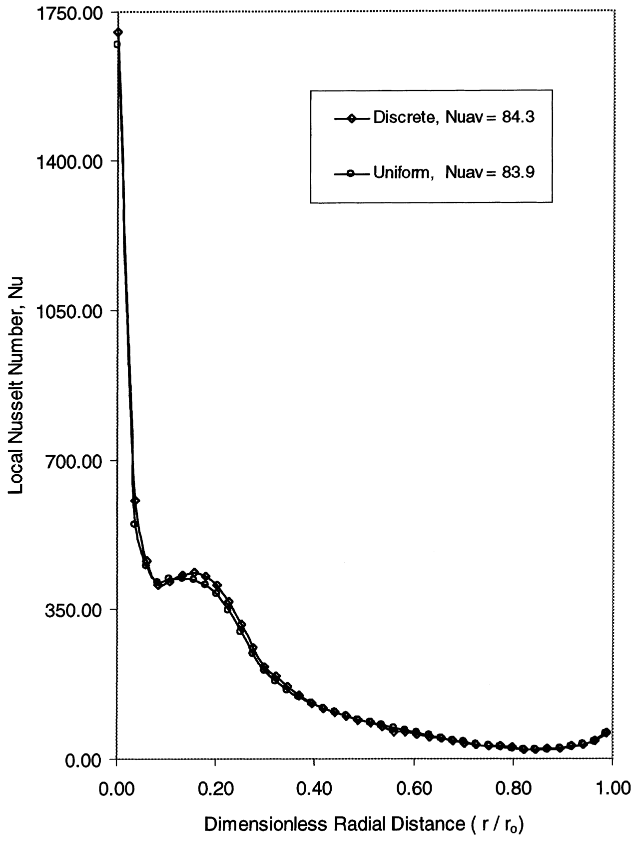

Fig. 17. Local Nusselt number for discrete (base case) and uniform heat flux distribution ($Re = 550$, $T_j = 348$ K, $b = 0.000125$ m, $H_n = 0.0085$ m, $r_n = 0.00085$ m, constantan plate, $q_0 = 1.59$ W).

respectively. It is noticed that a uniformly heated disk presents a more uniform temperature and the maximum temperature reached is lower. Since uniform and discrete heating had the same rate of total heat transfer, the heat flux at discrete heat sources was higher. This resulted in higher local temperature for the discrete source at the edge of the disk. The local Nusselt number plot shows that the discrete heat sources attain higher values due to the concentration of power; but as the fluid moves downstream, there is only slight difference between the two cases. The average Nusselt number for the discrete case is higher.

4. Conclusions

A theoretical model of conjugate heat transfer process where heat is transmitted through a solid body from discrete heat sources located on one side to a fluid jet impinging on the opposite side has been solved. The variation of fluid properties with temperature has been taken into account. It was found that the film thickness decreases as the impingement velocity increases. The heat transfer coefficient as well as the Nusselt number showed a strong dependence on the impingement velocity, increasing their values as the velocity increased. The temperature at the solid–fluid interface decreased as the velocity increased. The average Nusselt number increased with Reynolds number. As the thickness of the disk was increased, the heat transfer coefficient and the Nusselt number presented a thickness where they attained peak values, showing that there is an ideal disk thickness for best performance. The isothermal lines inside the solid showed that beyond a certain thickness, the disk presented a one-dimensional heat conduction in regions away from the impingement plane and the heated surface, and therefore discrete heat sources did not exert much influence on the convective heat transfer process. Similarly, the maximum temperature as well as the difference of maximum and minimum temperature at the interface was strongly affected by the variation of disk thickness at smaller thicknesses, but did not vary significantly at larger thicknesses. The thermal conductivity of the disk material strongly affected the magnitude of maximum temperature in the solid, temperature difference at the interface, heat transfer coefficient, as well as the Nusselt number. It was found that a lower thermal conductivity in the solid results in slightly higher heat transfer coefficient, whereas a higher thermal conductivity material will maintain the disk at a lower temperature. The location of the discrete heat sources affected the temperature distribution within the solid and consequently the average Nusselt number.

References

Besserman, D.L., Ramadhyani, S., Incropera, F.P., 1991. Numerical simulation of laminar flow and heat transfer for liquid jet impingement cooling of a circular heat source with annular collection of the spent fluid. Numerical Heat Transfer Part A 20, 263–278.

Burmeister, L.C., 1993. Convective Heat Transfer, 2nd ed. Wiley, New York.

Fletcher, C.A.J., 1984. Computational Galerkin Methods. Springer, New York.

Garimella, S.V., Rice, R.A., 1995. Confined and submerged liquid jet impingement heat transfer. J. Heat Transfer 117, 871–877.

Hrycak, P., 1983. Heat transfer from round impinging jets to a flat plate. Int. J. Heat and Mass Transfer 26 (12), 1857–1865.

Maddox, D.E., Bar-Cohen, A., 1994. Thermofluid design of single-phase submerged-jet impingement cooling for electronic components. J. Electronic Packaging 116, 237–240.

Martin, H., 1977. Heat and mass transfer between impinging gas jets and solid surfaces. Advances in Heat Transfer 13, 1–60.

Polat, S., Huang, B., Majumdar, A.S., Douglas, W.J.M., 1989. Numerical flow and heat transfer under impinging jets: a review. Annual Review of Numerical Fluid Mechanics and Heat Transfer 2, 157–197.

Rajaratnam, N., 1976. Turbulent Jets. Elsevier, New York.

Rice, R.A., Garimella, S.V., 1994. Heat transfer from discrete sources using an axisymmetric, submerged and confined liquid jet. In: Proceedings of the 10th International Heat Transfer Conference, vol. 3, Brighton, UK, pp. 89–94.

Rodi, W., 1982. Turbulent Buoyant Jets and Plumes. Pergamon, New York.

Schaffer, D., Incropera, F.P., Ramadhyani, S., 1991. Planar liquid jet impingement cooling of multiple discrete heat sources. J. Electronic Packaging 113, 359–366.

Vader, D.T., Incropera, F.P., Viskanta, R., 1991. Local convective heat transfer from a heated surface to an impinging, planar jet of water. Int. J. of Heat and Mass Transfer 34 (3), 611–623.

Wadsworth, D.C., Mudawar, I., 1990. Cooling of a multiple electronic module by means of confined two-dimensional jets of dielectric liquid. J. Heat Transfer 112, 891–898.

Wang, X.S., Dagan, Z., Jiji, L.M., 1990. Prediction of surface temperature and heat flux of a microelectronic chip with jet impingement cooling. J. Electronic Packaging 112, 57–62.

White, F.M., 1999. Fluid Mechanics, 4th ed. WCB/McGraw-Hill, New York.

Wolf, D.H., Viskanta, R., Incropera, F.P., 1990. Local convective heat transfer from a heated surface to a planar jet of water with non-uniform velocity profile. J. Heat Transfer 112, 899–905.

Womac, D.J., Ramadhyani, S., Incropera, F.P., 1993. Correlating equations for impingement cooling of small heat sources with single circular liquid jets. J. Heat Transfer 115, 106–115.

Womac, D.J., Incropera, F.P., Ramadhyani, S., 1994. Correlating equations for impingement cooling of small heat sources with multiple liquid jets. J. Heat Transfer 116, 482–486.